



Cite this: *Nanoscale*, 2018, **10**, 12003

Freestanding $\text{CoSeO}_3 \cdot \text{H}_2\text{O}$ nanoribbon/carbon nanotube composite paper for 2.4 V high-voltage, flexible, solid-state supercapacitors†

Yingchang Jiang, Zeyi Wu, Le Jiang, Zhichang Pan, Peiyu Yang, Wenchao Tian and Linfeng Hu *

The integration of high flexibility, high energy density and wide voltage window for solid-state supercapacitors remains a big challenge to date. Herein, ultrathin $\text{CoSeO}_3 \cdot \text{H}_2\text{O}$ nanoribbons (thickness: ~ 14 nm) with typical pseudocapacitive behavior were synthesized in a high yield by a solution-based refluxing process. Freestanding $\text{CoSeO}_3 \cdot \text{H}_2\text{O}$ ribbon/hydroxylated multi-walled carbon nanotube (HWCNT) paper could be fabricated through a vacuum-assisted filtration strategy owing to its ultrathin nature, ribbon-like morphology and inherent flexibility. Unexpectedly, an asymmetric supercapacitor constructed from this as-prepared $\text{CoSeO}_3 \cdot \text{H}_2\text{O}$ /HWCNT hybrid paper exhibits a high 2.4 V voltage window as well as excellent rate capability and cycle performance. The energy density of this device is $132.3 \text{ W h kg}^{-1}$ at 960 W kg^{-1} with a stable cycling ability of up to 10 000 cycles, which is superior to those of almost all previously reported asymmetric supercapacitors based on freestanding paper. Furthermore, this supercapacitor shows outstanding bendability and mechanical stability at different bending degrees from 0° to 180° with no changes in capacitive behavior. Our work provides new opportunities for developing high-performance asymmetric supercapacitors with high energy density, wide voltage window, and high flexibility in a novel $\text{CoSeO}_3 \cdot \text{H}_2\text{O}$ system for potential applications including flexible displays, collapsible mobile phones, and wearable equipment.

Received 11th April 2018,
Accepted 23rd May 2018
DOI: 10.1039/c8nr02924e
rsc.li/nanoscale

Introduction

The rapidly growing commercial markets of portable electronics and electric vehicles have stimulated an imperative requirement for high-performance energy storage devices.¹ Among various power sources, a supercapacitor is the most remarkable candidate due to its relatively simple structure and capability to bridge the gap between batteries and conventional capacitors with the desirable attributes of higher power density, fast charge/discharge, superior safety, outstanding cycling stability, environmental friendliness.^{2–4} In particular, the recently burgeoning growth of portable and wearable electronics has stimulated an imperative requirement for a new generation of flexible supercapacitors for their great potential applicability in powering the various prospective electronic products, for example, flexible displays, collapsible mobile phones, and many devices capable of being rolled up or twisted, including some wearable equipment.^{5,6} Therefore,

design and fabrication of flexible electrodes with excellent electrochemical performance and mechanical properties of being deformable have been arousing tremendous attention in recent years. Recently, freestanding paper made from low-dimensional nanomaterials through a facile vacuum-assisted filtration strategy has been widely developed as high-performance electrodes for flexible, foldable supercapacitors. Typically, a supercapacitor fabricated with large-area graphene paper exhibits high areal specific capacitance and can be bent to arbitrary angles.^{7,8} For example, high-quality MXene/carbon nanotube composite paper was rationally designed with high volumetric capacitance.⁹ A highly flexible and symmetric supercapacitor based on a novel $\text{MnO}_2/\text{Ti}_3\text{C}_2$ hybrid thin-film composed of molecularly stacked two-dimensional (2D) oxide and Ti_3C_2 nanosheets shows energy and power density of 8.3 W h kg^{-1} and 221.33 W kg^{-1} .¹⁰

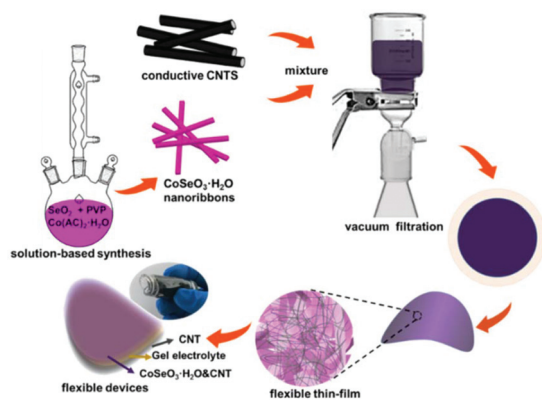
On the other hand, the energy density per unit of quantity or volume of electrochemical capacitors is still limited for practical applications. According to the equation of energy density $E = 1/2CV^2$, for a given supercapacitor, the energy density highly depends on the specific capacitance (C) and the operating voltage window (V).¹¹ Given by this equation, the energy density is proportional to the square of the operating

Department of Materials Science, Fudan University, Shanghai 200433, P. R. China.
E-mail: linfenghu@fudan.edu.cn

† Electronic supplementary information (ESI) available. See DOI: 10.1039/c8nr02924e

voltage window. Accordingly, to develop advanced supercapacitors with high energy densities, improving the capacitance and enlarging the operating voltage would be of equal importance. However, most of the previous research studies just focused on improving the specific capacitance of electrode materials.^{12–15} The limited voltage range around 1.0 V of supercapacitors based on aqueous electrolytes should be attributed to the water splitting at 1.23 V. By constructing an asymmetric supercapacitor configuration employing different electrode materials in the cathode and anode, the operating voltage of the supercapacitor can be increased to 1.5–1.8 V. Most recently, a 2.6 V aqueous asymmetric supercapacitor was found in $\text{Na}_{0.5}\text{MnO}_2$ nanosheet assembled nanowall arrays.¹⁶ Liu *et al.* also realized a 2.4 V high-voltage aqueous supercapacitor by rational design of a Ni–Mn–O solid-solution electrode.¹⁷ Although this important progress in advanced materials realizes the increase in the operating voltage, the combination of high flexibility, high energy density and wide voltage window for supercapacitors is rarely reported and remains a big challenge. Undoubtedly, the development of supercapacitors with wide voltage window, high energy density and excellent flexibility is highly desired.

Transition-metal selenides, including CoSe, $\text{Co}_{0.85}\text{Se}$, CoSe_2 , *etc.*, have attracted considerable attention and exhibit excellent performance in energy storage devices.^{18–22} Herein, we developed a PVP assisted solution-based refluxing process to prepare novel $\text{CoSeO}_3\cdot\text{H}_2\text{O}$ nanoribbons with a thickness of ~14 nm in a high yield. Interestingly, we found that a highly flexible paper made from these $\text{CoSeO}_3\cdot\text{H}_2\text{O}$ nanoribbons and hydroxylated multi-walled carbon nanotubes (HWCNTs) could be obtained by the vacuum-assisted filtration strategy (Scheme 1). Compared with other morphologies in the nanoscale (*e.g.* nanoparticles) for suction filtration into paper, this unique structure of the nanoribbon takes advantage of its ultrathin nature, high aspect ratio, ribbon-like morphology and inherent flexibility. Then, an all-solid-state asymmetric supercapacitor based on this freestanding $\text{CoSeO}_3\cdot\text{H}_2\text{O}$ /HWCNT paper exhibits amazing electrochemical performance



Scheme 1 Schematic illustration of the fabrication of the $\text{CoSeO}_3\cdot\text{H}_2\text{O}$ /HWCNT hybrid paper and the construction of a flexible supercapacitor from this paper.

with an operating voltage of 2.4 V and a high energy density of $132.3 \text{ W h kg}^{-1}$ at 960 W kg^{-1} , which is superior to all of the previously documented paper-based supercapacitors. Meanwhile, this energy storage device shows excellent flexibility with deformable mechanical properties with no significant performance change at bending angles from 0° to 180° .

Results and discussion

Synthesis and characterization of $\text{CoSeO}_3\cdot\text{H}_2\text{O}$ nanoribbons

Ultrathin $\text{CoSeO}_3\cdot\text{H}_2\text{O}$ nanoribbons were synthesized by a refluxing process of an aqueous solution consisting of $\text{Co}(\text{Ac})_2$ and SeO_2 with polyvinyl pyrrolidone (PVP) as the surfactant. Fig. 1a shows the XRD pattern of the as-prepared product, which can be indexed to a pure $\text{CoSeO}_3\cdot\text{H}_2\text{O}$ phase with a monoclinic structure (JCPDS no. 88-1510). The typical SEM image in Fig. 1b reveals numerous nanoribbon-like objects with lengths of several ten microns, and the bending appearance of these nanoribbons shows its inherent flexibility. Such a nanoribbon morphology was further confirmed by transmission electron microscopy (TEM) observation (Fig. 1c and d). The corresponding selected area electron diffraction (SAED) pattern taken from an individual nanoribbon displays very sharp diffraction spots with a rectangular pattern (Fig. 1e), confirming the high crystallinity of the as-synthesized sample. However, the sample is metastable under high voltage e-beam irradiation and it was very difficult to get the high-resolution transmission electron microscopy (HRTEM) image. The nano-

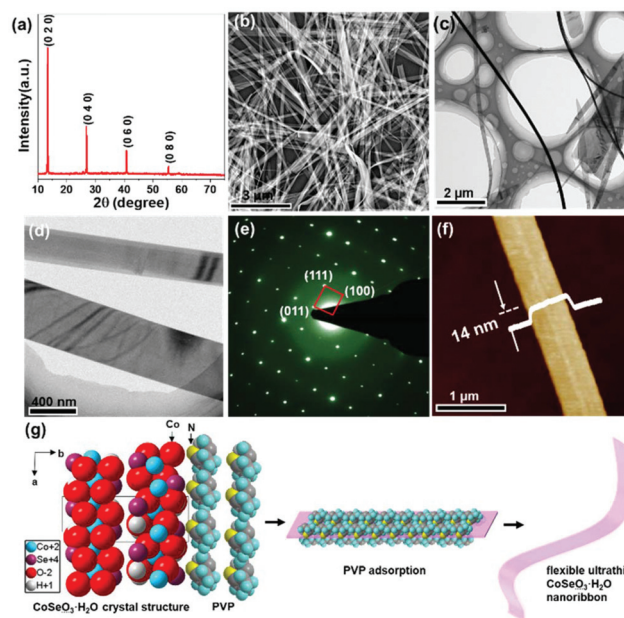


Fig. 1 (a) XRD pattern of the as-prepared $\text{CoSeO}_3\cdot\text{H}_2\text{O}$ sample. Typical (b) SEM, (c) and (d) TEM images, and (e) SAED pattern taken from an individual $\text{CoSeO}_3\cdot\text{H}_2\text{O}$ nanoribbon. (f) AFM image and height information of the $\text{CoSeO}_3\cdot\text{H}_2\text{O}$ nanoribbons. (g) Schematic illustration of the growth of $\text{CoSeO}_3\cdot\text{H}_2\text{O}$ ultrathin nanoribbons.

ribbon gradually lost its high crystallinity and transformed to an amorphous structure with several broadened diffraction rings under these conditions (Fig. S1, ESI†). Note that the ribbons are semitransparent under TEM observation, indicating that an e-beam can penetrate the sample due to its ultrathin nature. The thickness of the as-obtained $\text{CoSeO}_3 \cdot \text{H}_2\text{O}$ nanoribbons was accurately examined to be as thin as ~ 14 nm by tapping-mode atomic force microscopy (AFM) characterization (Fig. 1f). Note that the addition of PVP in the starting reactant plays a key role in the formation of the ultrathin nanoribbons. In the absence of PVP, $\text{CoSeO}_3 \cdot \text{H}_2\text{O}$ crystals with an irregular one-dimensional shape and a length of several hundred micrometers were produced (Fig. S2, ESI†). Accordingly, as schematically illustrated in Fig. 1g, the PVP molecules might be adsorbed on the $\text{CoSeO}_3 \cdot \text{H}_2\text{O}$ ribbon surface, stabilize the $\text{CoSeO}_3 \cdot \text{H}_2\text{O}$ crystal nucleus and reduce the diffusion rate of reactive ions, leading to the growth of the ultrathin ribbon structure.^{23,24} Then, the PVP molecules on the nanoribbon surface can be completely removed by a following washing procedure with ethanol several times.

Electrochemical properties of the $\text{CoSeO}_3 \cdot \text{H}_2\text{O}$ /HWCNT free-standing paper

Fig. 2a shows the optical images of an aqueous dispersion of the as-grown $\text{CoSeO}_3 \cdot \text{H}_2\text{O}$ nanoribbons, appearing in pink color with the observation of a strong Tyndall scattering effect. We consider that its ultrathin nature, nanoribbon-like morphology and inherent flexibility are quite promising for fabricating freestanding paper by a facile vacuum-assisted filtration strategy. Expectedly, the $\text{CoSeO}_3 \cdot \text{H}_2\text{O}$ films are easily detachable from the filter membranes, resulting in free-standing paper with a pink color (Fig. S3, ESI†). On the other hand, taking advantage of the high conductivity of HWCNTs, the inclusion of HWCNTs in this paper would greatly improve the conductivity. Accordingly, two colloidal aqueous solutions of $\text{CoSeO}_3 \cdot \text{H}_2\text{O}$ nanoribbons and HWCNTs were mixed together as shown in Fig. 2a (optimal mass ratio: $\text{CoSeO}_3 \cdot \text{H}_2\text{O}$:HWCNTs = 90:10). Subsequently, vacuum-assisted filtration of this mixed colloidal solution resulted in free-standing paper with a grey pink color (Fig. 2b), and it could be freely rolled up by hand and glass rods (Fig. S4, ESI†). The XRD characterization of this $\text{CoSeO}_3 \cdot \text{H}_2\text{O}$ /HWCNT paper-like sample shows a pattern similar to the pure $\text{CoSeO}_3 \cdot \text{H}_2\text{O}$ powder except a characteristic, broad peak of carbon nanotubes at $2\theta = 26^\circ$ (Fig. S5, ESI†). Note that the diffraction pattern showed intense and sharp (0 1 0) diffraction peaks, suggesting a preferred orientation along the [010] direction of $\text{CoSeO}_3 \cdot \text{H}_2\text{O}$ ribbons in this hybrid paper. The preferred orientation should be attributed to the high aspect ratio and ultrathin nature of our $\text{CoSeO}_3 \cdot \text{H}_2\text{O}$ nanoribbons. The typical SEM image of this paper sample in Fig. 2c indicates that HWCNTs were uniformly dispersed in the $\text{CoSeO}_3 \cdot \text{H}_2\text{O}$ nanoribbon matrix to form a nanonet like structure. Fig. 2d shows the corresponding local elemental maps, which demonstrates that Co, Se, O, C elements are homogeneously distributed in the sample. The cross-section SEM

image in Fig. 2e suggests that the thickness of this freestanding paper ranges from 30 to 40 μm . Followed by an electric measurement based on the four-point probe method, the electronic conductivities of $\text{CoSeO}_3 \cdot \text{H}_2\text{O}$ paper and $\text{CoSeO}_3 \cdot \text{H}_2\text{O}$ /HWCNT hybrid paper with different HWCNT weight ratios are summarized in Fig. S6, ESI†. No current signal for $\text{CoSeO}_3 \cdot \text{H}_2\text{O}$ paper was detected due to its intrinsic insulating property, which was revealed in our most recent work.²⁵ After the introduction of HWCNTs (mass ratio: $\text{CoSeO}_3 \cdot \text{H}_2\text{O}$:HWCNTs = 9:1), the intertwined networks of the $\text{CoSeO}_3 \cdot \text{H}_2\text{O}$ /HWCNT composite exhibit a greatly improved conductivity of upto 2.67 S cm^{-1} . Further increasing the HWCNT content in the hybrid paper (8:1) gives rise to a slight decrease of the conductivity (Fig. S6, ESI†). It might be attributed to the fact the carbon nanotubes at high concentrations are easy to aggregate together in the suction filter process (Fig. S7, ESI†). Furthermore, the high content of HWCNTs in this hybrid paper also leads to a decrease in the mechanical properties, as evident from the typical stress-strain curves of the hybrid papers at different $\text{CoSeO}_3 \cdot \text{H}_2\text{O}$:HWCNT weight ratios (Fig. S8, ESI†). Accordingly, the optimal mass ratio to fabricate a high-quality $\text{CoSeO}_3 \cdot \text{H}_2\text{O}$ /HWCNT hybrid paper should be 9:1. At this optimized weight ratio, the inserted HWCNTs greatly improve the conductivity of the paper sample with no significant breakdown of its mechanical strength.

We tried to evaluate the electrochemical properties of the $\text{CoSeO}_3 \cdot \text{H}_2\text{O}$ /HWCNT hybrid paper in a three-electrode cell configuration with a 1.0 M KOH solution as the electrolyte. However, this hybrid paper is not stable in the KOH aqueous solution and gradually converts into loose $\text{CoSeO}_3 \cdot \text{H}_2\text{O}$ and HWCNT powder due to the lack of any polymeric binder. Instead, a powder sample with the same composition as this hybrid paper was prepared and pressed onto nickel foam current collectors as the working electrode (average value of loading density: 3 mg cm^{-2} , measured carefully three times). Fig. 3a shows the representative cyclic voltammetry (CV) curves recorded at different scan rates ranging from 1 to 50 mV s^{-1} . The nonrectangular nature of the CV curve indicates that faradaic reversible reactions occur, confirming the obvious pseudocapacitive nature of the $\text{CoSeO}_3 \cdot \text{H}_2\text{O}$ electrode with well-defined redox peaks within -0.1 to 0.7 V (vs. SEC) . Three pairs of redox peaks due to the reversible reactions of $\text{Co(II)} \leftrightarrow \text{Co(III)}$, $\text{Co(III)} \leftrightarrow \text{Co(IV)}$ and $\text{Se(IV)} \leftrightarrow \text{Se(VI)}$ can be clearly seen.

The charge-discharge characteristics in Fig. 3b at different current densities from 5.0 to 50.0 A g^{-1} exhibit a quite clear deviation from the linear charge-discharge characteristic feature for an electric double layer capacitor, indicating the pseudocapacitive characteristic of the $\text{CoSeO}_3 \cdot \text{H}_2\text{O}$ nanoribbons resulting from redox reactions by adsorption or desorption of hydroxyl ions at the interface between the paper-like electrode and the liquid electrolyte. The charge-discharge curve is extremely symmetric with a coulombic efficiency of 98%, suggesting the highly reversible electrochemical behavior. Areal capacitance values were calculated as 2461, 2201, 2028, 1733, 1560, 1386 and 1213 F g^{-1} at current density

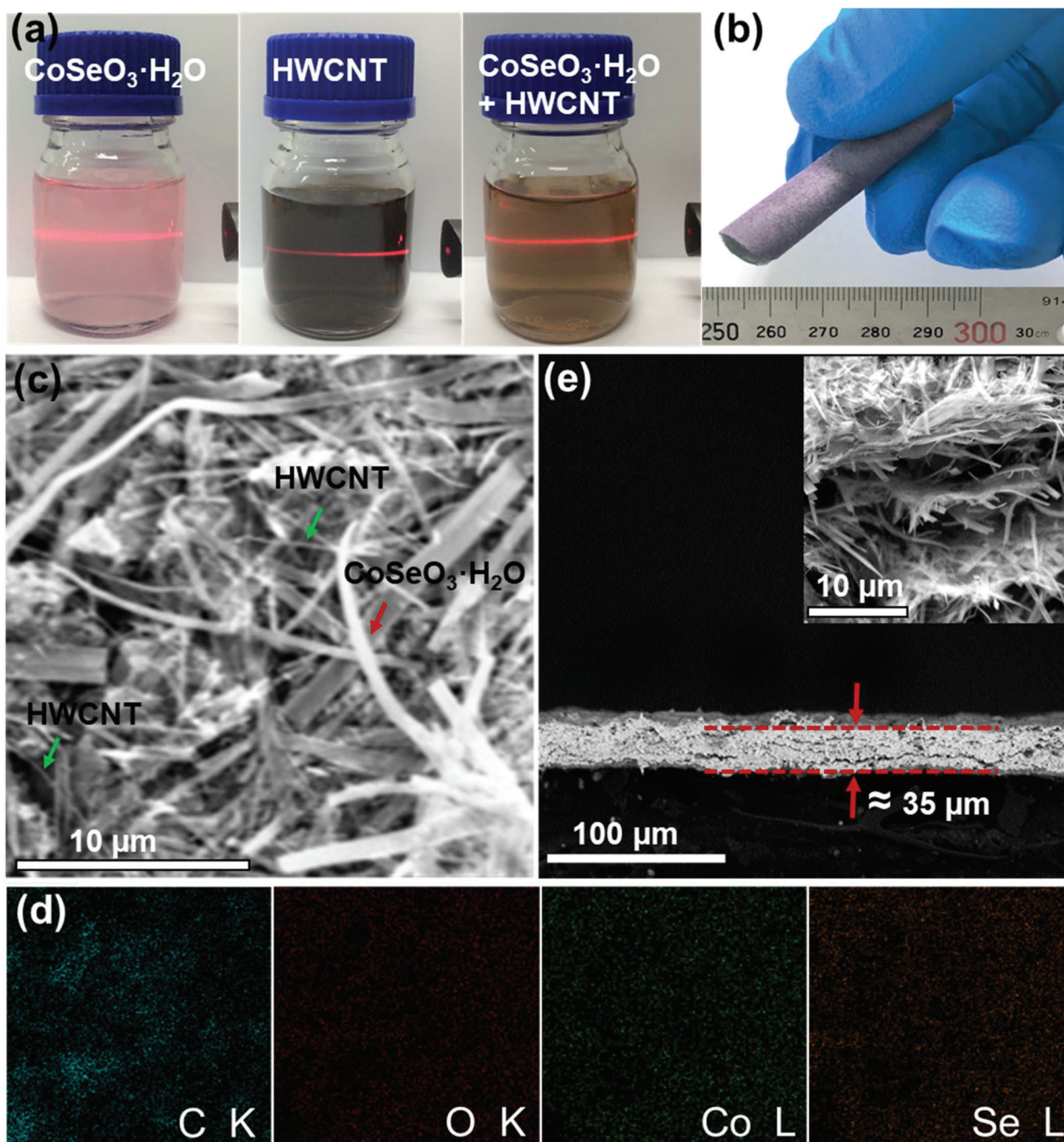


Fig. 2 (a) Digital photographs of $\text{CoSeO}_3 \cdot \text{H}_2\text{O}$, HWCNT, and $\text{CoSeO}_3 \cdot \text{H}_2\text{O}$, HWCNT mixture colloid suspensions, all displaying an obvious Tyndall scattering effect. (b) The digital photograph of the as-prepared $\text{CoSeO}_3 \cdot \text{H}_2\text{O}$ /HWCNT paper. (c) The in-plane SEM image and (d) the corresponding EDS elemental mapping results for Co, Se, O, and C elements. (e) The cross-section SEM image of the hybrid $\text{CoSeO}_3 \cdot \text{H}_2\text{O}$ /HWCNT paper.

values of 5, 10, 15, 20, 30, 40 and 50 A g^{-1} , respectively. Distinctly, this value exceeds that of previously reported Co, Ni oxides/hydroxides (Fig. 3c).^{26–33} The cycling stability of the material was examined up to 10 000 cycles with $\sim 86.2\%$ of capacitance retention at a high current density of 20.0 A g^{-1} , demonstrating its long-term stability and durability (Fig. 3d). From the Nyquist plots for the cobalt selenide case for the initial cycle and after 10 000 cycles (Fig. S9, ESI[†]), the longer

Warburg line in the low-frequency region after 10 000 cycles indicates the faster electrolyte diffusion into the electrode material compared with the initial cycle. The equivalent series resistance at the initial state is 2.43Ω and drops to 2.27Ω after 10 000 cycles. The smaller semicircle in the high-frequency region after cycling clearly shows lower charge transfer resistance at the electrode/electrolyte interface than that in the initial cycle.

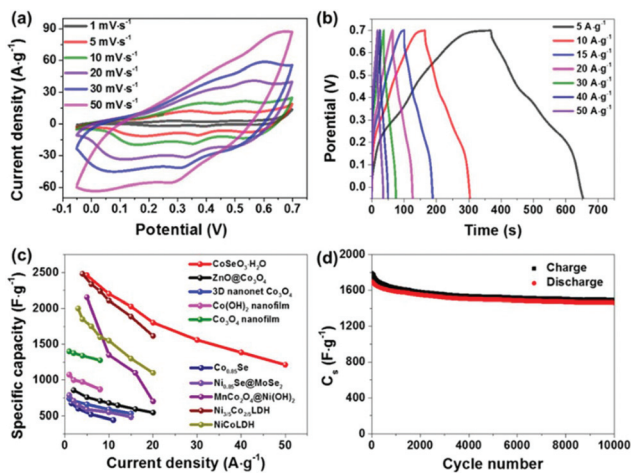


Fig. 3 (a) CV curves and (b) galvanostatic charge–discharge curves of the $\text{CoSeO}_3\cdot\text{H}_2\text{O}/\text{HWCNT}$ powder on Ni foam. (c) C_s of the electrode at different current densities and comparison with that of Co, Ni oxides/hydroxides. (d) Cycling performance of the electrode at a current density of 20.0 A g^{-1} .

Asymmetric supercapacitor based on $\text{CoSeO}_3\cdot\text{H}_2\text{O}/\text{HWCNT}$ hybrid paper

To construct an asymmetric supercapacitor, pure HWCNT paper was fabricated using the vacuum-assisted filtration strategy from a colloidal HWCNT suspension as shown in Fig. 2a. The morphology and electrochemical characterization of this HWCNT paper are shown in Fig. S10 and 11 ESI,† respectively. Finally, an asymmetric supercapacitor (ASC) was fabricated in a two-paper system with as-prepared $\text{CoSeO}_3\cdot\text{H}_2\text{O}/\text{HWCNT}$ hybrid paper as the positive electrode, HWCNT paper as the negative one and PVA-KOH gel electrolyte sandwiched between the electrodes (Fig. 4a). In this quasi-solid state case, the as-prepared paper samples were stable in the PVA-KOH gel electrolyte. The CV curve of this ASC exhibits apparent redox peaks originating from the pseudocapacitive behavior of the $\text{CoSeO}_3\cdot\text{H}_2\text{O}$ nanoribbons (Fig. 4b). The current increased with increasing scan rates, and the shape was well maintained even at a scan rate up to 50 mV s^{-1} . This CV curve is quite different from that of pure HWCNT paper electrodes, demonstrating the double contribution of the electric double-layer capacitance from the HWCNTs and the pseudocapacitance from the $\text{CoSeO}_3\cdot\text{H}_2\text{O}$ nanoribbons, respectively. Unexpectedly and importantly, the operating potential window of the present device is up to 2.4 V.

Note that the potential windows of 0–0.7 V for $\text{CoSeO}_3\cdot\text{H}_2\text{O}$ @Ni foam and –1.0 to 0 V for HWCNTs@Ni foam were obtained in the three-electrode cell configuration using a 1.0 M KOH aqueous solution as the electrolyte (Fig. S12, ESI†). However, it is strange that the resulting $\text{CoSeO}_3\cdot\text{H}_2\text{O}$, HWCNT//PVA-KOH//HWCNT device achieves a wide operating potential window of up to 2.4 V.

We consider that our $\text{CoSeO}_3\cdot\text{H}_2\text{O}$ sample might exhibit an intrinsically wide potential window of up to 0–1.4 V in an

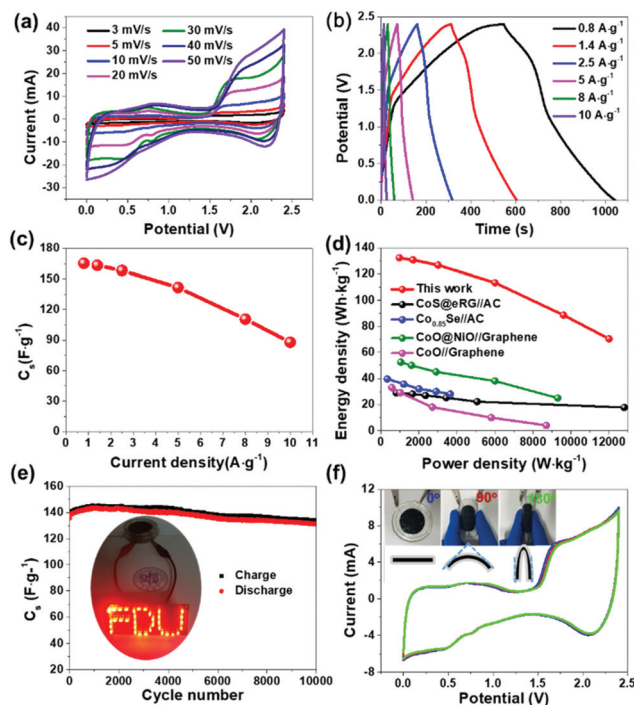


Fig. 4 (a) CV curves of the $\text{CoSeO}_3\cdot\text{H}_2\text{O}$, HWCNT//PVA-KOH//HWCNT asymmetric supercapacitor at different scan rates. (b) Galvanostatic charge–discharge curves and (c) C_s of this asymmetric supercapacitor at different current densities. (d) Ragone plot related to energy and power densities of some reported cobalt or selenium based composites as anode materials and the present work. All data in this figure are based on the total mass of both electrodes. (e) Cycling performances during 10 000 cycles at a current density of 5 A g^{-1} (inset: image of the LED panel powered by three charged asymmetric supercapacitors in series). (f) Flexibility and stability of the asymmetric supercapacitor upon flexing evaluated by measuring CV curves at different bending angles.

aqueous environment. However, we cannot carry out this measurement due to the following reasons:

(1) In the three-electrode cell configuration using the water electrolyte, the potential window generally cannot exceed 1.2 V due to the water decomposition when the voltage is higher than this threshold value.¹⁴

(2) The electrocatalytic effect from the Ni foam substrate: the hybrid paper electrode was not strong enough and gradually broke up in the KOH aqueous solution. It cannot be directly used as an electrode in the three-electrode system. Alternatively, the active $\text{CoSeO}_3\cdot\text{H}_2\text{O}$ powder was coated on the Ni foam for the test. According to the previous study, the potential window of the electrode is generally lower than 0.8 V using Ti, Ni metal substrates as current collectors due to the Ti, Ni electrocatalytic effect.¹⁴

When the paper-based electrode was assembled into an all-solid-state supercapacitor using a PVA-KOH gel electrolyte, the above constraints on water decomposition disappeared. Accordingly, a higher potential window of up to 0–1.4 V can be detected in our $\text{CoSeO}_3\cdot\text{H}_2\text{O}/\text{HWCNT}$ paper, and the resulting $\text{CoSeO}_3\cdot\text{H}_2\text{O}$, HWCNT//PVA-KOH//HWCNT devices show a wide operating potential window of up to 2.4 V.

The charge–discharge performance of the device was further evaluated up to 2.4 V for the applied current densities from 0.8 to 10 A g⁻¹, displayed in Fig. 4c. The capacitance value of 165 F g⁻¹ at a current density value of 0.8 A g⁻¹ evaluated from the total mass including both the positive and negative electrodes is superior to those of most other asymmetric supercapacitors recently reported. Even with the current density increasing to 10.0 A g⁻¹, the asymmetric supercapacitor still showed a high specific capacitance of 96.25 F g⁻¹, which should originate from the high electrochemically active surface area and efficient mass transportation of the constructed netlike structure. The Ragone diagram depicts the plot of the energy and power densities of the fabricated device, which were attained from the calculation based on the galvanostatic discharge plots (Fig. 4d). At 2.4 V, the as-fabricated asymmetric supercapacitor exhibits an energy density of 132.3 W h kg⁻¹ at a power density of 960 W kg⁻¹, and still maintains 77 W h kg⁻¹ at 13 137.4 W kg⁻¹. Fig. 4d and Table S1 (ESI†) compare the performance metrics of our device and various previously documented asymmetric supercapacitors.^{34–40} The energy density (132.3 W h kg⁻¹) in this work, to the best of our knowledge, is the highest value among all freestanding paper-based asymmetric flexible ASCs recently reported. These amazing electrochemical properties of our CoSeO₃·H₂O/HWCNT paper should be attributed to the good conductivity, high surface areas accessible to ions, intrinsically high voltage window and mechanical robustness of the hybrid paper.

The long-term cycling performance of the CoSeO₃·H₂O, HWCNT//PVA-KOH//HWCNT devices was evaluated in the voltage window of 0–2.4 V at 5 A g⁻¹ (Fig. 4e). This ASC exhibits a capacitance retention of 94% after 10 000 charging/discharging cycles. Such a cycling and retention performance is significantly superior to those of other ASCs recently reported, such as MnO₂/graphene//CNT/graphene (84.4% retention after 10 000 cycles),³⁶ graphene/MnO₂//graphene (79% retention after 1 000 cycles),⁴¹ NiSe@MoSe₂//N-PMCN ASC (91% retention after 5 000 cycles),³¹ and HWCNTs@Ni(OH)₂//AC (83% retention after 3 000 cycles).⁴² The asymmetric supercapacitors were further assembled in series to validate their practical application (inset in Fig. 4e). When three as-prepared supercapacitors were connected in series, after charging up to 7.2 V, the large-sized tandem supercapacitors can efficiently power a well-designed 36 light-emitting diode (LED) indicator arrays (open circuit voltage: 4.76 V).

Considering the intrinsic flexibility of the freestanding CoSeO₃·H₂O/HWCNT paper, the as-fabricated asymmetric CoSeO₃·H₂O, HWCNT//PVA-KOH//HWCNT supercapacitor would show excellent flexibility. In order to demonstrate the flexibility and stretchability, we measured the CV curves at the scan rate of 10 mV s⁻¹ at different bending degrees of 0°, 90°, and 180°. The as-obtained CV curves showed no significant changes, manifesting outstanding bendability and mechanical stability of the device during folding (Fig. 4f).

Conclusions

In summary, we reported a facile refluxing process to synthesize ultrathin CoSeO₃·H₂O nanoribbons, which were used as ideal building blocks for a hybrid, freestanding CoSeO₃·H₂O/HWCNT paper owing to the ultrathin nature, ribbon-like morphology and inherent flexibility. Impressively and unexpectedly, the as-fabricated CoSeO₃·H₂O, HWCNT//PVA-KOH//HWCNT solid-state supercapacitor exhibits a 2.4 V voltage window. The energy density of this device was estimated as 132.3 W h kg⁻¹ with a very stable cycling ability up to 10 000 cycles, outperforming all freestanding paper-based asymmetric flexible ASCs recently reported. The present study demonstrates the possibility of the integration of high flexibility, high energy density and wide voltage window for solid-state supercapacitors in a novel CoSeO₃·H₂O nanoribbon system. The as-obtained freestanding CoSeO₃·H₂O/HWCNT paper would also show promising performances in other electrochemical energy storage devices, such as lithium (sodium)-ion batteries, air batteries, and electrochemical actuators.

The electrochemical performance of a CoSeO₃ sample without crystalline water is also being studied.

Experimental

Materials

All the reagents were of AR grade and were used without further purification. Double distilled water (18.2 MΩ) was used throughout the course of the reaction. Hydroxylated multi-walled carbon nanotubes (inner diameter: 5–10 nm, outer diameter: 10–20 nm, length: 10–30 μm) were purchased from Jiangsu HENGQIU Materials Tech Co., Ltd. Co(Ac)₂·4H₂O, SeO₂, KOH, CTAB (hexadecyltrimethylammonium bromide) and PVP (K-30) were purchased from Sinopharm Chemical Reagent Co., Ltd.

Synthesis of CoSeO₃·H₂O nanoribbons

CoSeO₃·H₂O nanoribbons were synthesized by a solution-based refluxing method. Briefly, 3.0 g of PVP (K-30) was dissolved in 700 mL of deionized water under magnetic stirring. Co(Ac)₂·4H₂O (1.4 mmol) and SeO₂ (1.4 mmol) were added into the above aqueous solution in succession under drastic stirring. The dispersion was refluxed under continuous magnetic stirring and nitrogen gas protection at 120 °C for 6 h. Upon cooling to room temperature, the product was washed with deionized water and ethanol several times to completely remove the PVP surfactant, and dried under vacuum at 70 °C for further analysis.

Fabrication of CoSeO₃·H₂O/HWCNT paper

The CoSeO₃·H₂O/HWCNTs and HWCNT paper-like samples were prepared by vacuum-filtration assembly. The CoSeO₃·H₂O and HWCNT powder was fully dispersed in the mixed solvent of ethylene glycol and water with a concentration of

50 mg mL⁻¹ for each component. Then, the as-obtained suspension was vacuum filtered onto a mixed cellulose membrane with a 0.22 μm pore size (Sinopharm Chemical Reagent Co., Ltd), forming a homogeneous pure CoSeO₃·H₂O or HWCNT thin-film on the membrane. For the CoSeO₃·H₂O/HWCNT hybrid paper, it was prepared by just mixing two suspensions with different mass ratios before suction filtering. After drying in air, they could be facily stripped from the filter membrane by hand.

Fabrication of CoSeO₃·H₂O/HWCNT paper for solid-state asymmetric supercapacitors (ASCs)

The solid-state ASCs were assembled by separating the CoSeO₃·H₂O/HWCNT and HWCNT paper-like electrodes with normal filter paper. PVA/KOH gel was used as the electrolyte and prepared by mixing 8.0 g of PVA and 8.0 g of KOH in 100 mL of deionized water, and heated at 80 °C for 12 h under vigorous stirring. Before assembling, one piece of CoSeO₃·H₂O/HWCNT paper (diameter: 4 cm, mass: ≈1 g) and one piece of HWCNT paper (diameter: 4 cm) were soaked in PVA/KOH for 2 h. The flexible solid-state supercapacitor was encapsulated with silicone after the gel electrolyte solidified at room temperature.

Materials characterization

Sample morphologies were characterized using a FEI Nano SEM 450 field-emission scanning electron microscope (SEM) and a Bruker Dimension Icon atomic force microscope (AFM). Transmission electron microscopy (TEM), high-resolution microscopy (HRTEM) and selected area electron diffraction (SAED) were performed using a Philips CM 200 FEG field emission microscope at an acceleration voltage of 300 kV. The crystal structure characteristics were studied using a Bruker D8-A25 diffractometer with Cu Kα radiation (λ = 1.5406 Å). The electric conductivity of composite paper was determined by a four-probe method (b1500A, Agilent Co., Ltd) under a sample platform equipped with parallel probes (probe spacing: 1 mm). The tensile properties of the as-obtained papers were measured using a PARAM XLW(PC) instrument at room temperature with a humidity of about 25%.

Electrochemical measurements

For three-electrode cell measurement, the nickel foam supporting active materials (loading mass: ≈3 mg cm⁻²) acted directly as the working electrodes and were soaked in a 1 M KOH solution and degassed under vacuum for 1 h before the electrochemical test. Active CoSeO₃·H₂O powder, multi-walled carbon nanotubes (conductor) and binder (polyvinylidene fluoride, PVDF) were mixed in a weight ratio of 81 : 9 : 10; an anhydrous ethanol solvent was added to form slurry. The well-mixed slurry was coated onto a Ni foam as a current collector and then dried under vacuum at 60 °C for 12 h. The mass loading of the active compound on the Ni foam was determined by subtracting the weight before and after the coating, and this measurement was carried out three times to eliminate experimental errors. The electrochemical properties of the as-

obtained electrodes were investigated under a three-electrode cell configuration at 25 °C in 1 M KOH. Platinum foil and an Ag/AgCl electrode were used as the counter and reference electrodes, respectively.

The electrochemical properties of the asymmetric supercapacitor were investigated under a two-electrode cell configuration with the CoSeO₃·H₂O electrode as the positive electrode and the HWCNT electrode as the negative electrode with a gel electrolyte. The CV, galvanostatic charge–discharge, and electrochemical impedance spectroscopy (EIS) measurements were conducted on a Gamary 90I electrochemical workstation (Gamary Instrument Company, USA). Capacitance balance was done for both electrodes according to their corresponding capacitances and masses ($m_{\text{cathode}} \times C_{\text{s-cathode}} = m_{\text{anode}} \times C_{\text{s-anode}}$).

Conflicts of interest

The authors declare no conflict of interest.

Acknowledgements

This work was financially supported by the National Natural Science Foundation of China (No. 51701042 and 51372040) the Shanghai Rising-Star Program (16QA1400700).

References

- 1 J. M. Tarascon and M. Armand, *Nature*, 2001, **414**, 359–367.
- 2 J. M. Luo, W. K. Zhang, H. D. Yuan, C. B. Jin, L. Y. Huang, C. Liang, Y. Xia, J. Zhang, Y. P. Gan and X. Y. Tao, *ACS Nano*, 2017, **11**, 2459.
- 3 R. Ma, X. H. Liu, J. B. Liang, Y. Bando and T. Sasaki, *Adv. Mater.*, 2014, **26**, 4173.
- 4 X. H. Liu, R. Ma, Y. Bando and T. Sasaki, *Angew. Chem., Int. Ed.*, 2010, **49**, 8253.
- 5 Y. Huang, M. Zhong, Y. Huang, M. Zhu, Z. Pei, Z. Wang, Q. Xue, X. Xie and C. Zhi, *Nat. Commun.*, 2015, **6**, 10310.
- 6 Y. Huang, M. Hong, F. Shi, X. Liu, Z. Tang, Y. Wang, Y. Huang, H. Hou, X. Xie and C. Zhi, *Angew. Chem., Int. Ed.*, 2017, **56**, 9141.
- 7 L. L. Liu, Z. Q. Niu, L. Zhang, W. Y. Zhou, X. D. Chen and S. S. Xie, *Adv. Mater.*, 2014, **26**, 4855–1862.
- 8 Z. Y. Xiong, C. L. Liao, W. H. Han and X. G. Wang, *Adv. Mater.*, 2015, **27**, 4469–4475.
- 9 M. Q. Zhao, C. E. Ren, Z. Ling, M. R. Lukatskaya, C. F. Zhang, K. L. Van Aken, M. W. Barsoum and Y. Gogotsi, *Adv. Mater.*, 2015, **27**, 339–345.
- 10 W. H. Liu, Z. Q. Wang, Y. L. Su, Q. W. Li, Z. G. Zhao and F. X. Geng, *Adv. Energy Mater.*, 2017, **7**, 1602834.
- 11 L. X. Feng, K. Wang, X. Zhang, X. Z. Sun, C. Li, X. B. Ge and Y. W. Ma, *Adv. Funct. Mater.*, 2017, 1704463.
- 12 D. P. Qi, Y. Liu, Z. Y. Liu, L. Zhang and X. D. Chen, *Adv. Mater.*, 2017, **29**, 1602802.

- 13 Y. F. Bu, T. Sun, Y. J. Cai, L. Y. Du, O. Zhuo, L. J. Yang, Q. Wu, X. Z. Wang and Z. Hu, *Adv. Mater.*, 2017, **29**, 1700470.
- 14 J. L. Kang, A. Hirata, H. J. Qiu, L. Y. Chen, X. B. Ge, T. Fujita and M. W. Chen, *Adv. Mater.*, 2014, **26**, 269–272.
- 15 M. Ghidui, M. R. Lukatskaya, M. Q. Zhao, Y. Gogotsi and M. W. Barsoum, *Nature*, 2014, **516**, 78–81.
- 16 N. Jabeen, A. Hussain, Q. Y. Xia, S. Sun, J. W. Zhu and H. Xia, *Adv. Mater.*, 2017, **29**, 1700804.
- 17 W. H. Zuo, C. Y. Xie, P. Xu, Y. Y. Li and J. P. Liu, *Adv. Mater.*, 2017, **29**, 1703463.
- 18 A. Banerjee, S. Bhatnagar, K. K. Upadhyay, P. Yadav and S. Ogale, *ACS Appl. Mater. Interfaces*, 2014, **6**, 18844–18852.
- 19 X. F. Wang, B. Liu, Q. F. Wang, W. F. Song, X. J. Hou, D. Chen, Y. B. Cheng and G. Z. Shen, *Adv. Mater.*, 2013, **25**, 1479–1486.
- 20 Z. Li, H. Xue, J. Wang, Y. Tang, C. S. Lee and S. Yang, *ChemElectroChem*, 2015, **2**, 1682–1686.
- 21 Y. F. Shi, C. X. Hua, B. Li, X. P. Fang, C. H. Yao, Y. C. Zhang, Y. S. Hu, Z. X. Wang, L. Q. Chen, D. Y. Zhao and G. D. Stucky, *Adv. Funct. Mater.*, 2013, **23**, 1832–1838.
- 22 Y. Zhao, X. F. Li, B. Yan, D. B. Xiong, D. J. Li, S. Lawes and X. L. Sun, *Adv. Energy Mater.*, 2016, **6**, 1502175.
- 23 H. Tsunoyamam and T. Tsukuda, *J. Am. Chem. Soc.*, 2009, **131**, 18216–18217.
- 24 G. Collins, M. Schmidt, G. P. McGlacken, C. Dwyer and J. D. Holmes, *J. Phys. Chem. C*, 2014, **118**, 6522–6530.
- 25 Y. C. Jiang, Y. Song, Z. C. Pan, Y. Meng, L. Jiang, Z. Y. Wu, P. Y. Yang, Q. F. Gu, D. L. Sun and L. F. Hu, *ACS Nano*, 2018, **12**, 5011–5020.
- 26 D. P. Cai, H. Huang, D. D. Wang, B. Liu, L. L. Wang, Y. Liu, Q. H. Li and T. H. Wang, *ACS Appl. Mater. Interfaces*, 2014, **6**, 15905–15912.
- 27 D. N. Lan, Y. Y. Chen, P. Chen, X. Y. Chen, X. Wu, X. L. Pu, Y. Zeng and Z. H. Zhu, *ACS Appl. Mater. Interfaces*, 2014, **6**, 11839–11845.
- 28 L. Wang, C. Lin, F. X. Zhang and J. Jin, *ACS Nano*, 2014, **8**, 3724–3734.
- 29 C. Feng, J. F. Zhang, Y. He, C. Zhong, W. B. Hu, L. Liu and Y. D. Deng, *ACS Nano*, 2015, **9**, 1730–1739.
- 30 C. Gong, M. L. Huang, P. Zhou, Z. X. Sun, L. Q. Fan, J. M. Lin and J. H. Wu, *Appl. Surf. Sci.*, 2016, **362**, 469–476.
- 31 H. Peng, J. Z. Zhou, K. J. Sun, G. F. Ma, Z. G. Zhang, E. Feng and Z. Q. Lei, *ACS Sustainable Chem. Eng.*, 2017, **5**, 5951–5963.
- 32 Y. Zhao, L. F. Hu, S. Y. Zhao and L. M. Wu, *Adv. Funct. Mater.*, 2016, **26**, 4085–4093.
- 33 H. Chen, L. F. Hu, M. Chen, Y. Yan and L. M. Wu, *Adv. Funct. Mater.*, 2014, **24**, 934–942.
- 34 Z. Gao, N. N. Song and X. D. Li, *J. Mater. Chem. A*, 2015, **3**, 14833–14844.
- 35 N. Liu, Y. L. Su, Z. Q. Wang, Z. Wang, J. S. Xia, Y. Chen, Z. G. Zhao, Q. W. Li and F. X. Geng, *ACS Nano*, 2017, **11**, 7879–7888.
- 36 Z. Y. Zhang, F. Xiao, L. H. Qian, J. W. Xiao, S. Wang and Y. Q. Liu, *Adv. Energy Mater.*, 2014, **4**, 1400064.
- 37 Q. Q. Ke, C. Guan, X. Zhang, M. R. Zheng, Y. W. Zhang, Y. Q. Cai, H. Zhang and J. Wang, *Adv. Mater.*, 2017, **29**, 1604164.
- 38 J. W. Zhao, J. L. Chen, S. M. Xu, M. F. Shao, Q. Zhang, F. Wei, J. Ma, M. Wei, D. G. Evans and X. Duan, *Adv. Funct. Mater.*, 2014, **24**, 2938–2946.
- 39 Z. Gao, W. L. Yang, J. Wang, N. N. Song and X. D. Li, *Nano Energy*, 2015, **13**, 306–317.
- 40 B. G. Choi, S. J. Chang, H. W. Kang, C. P. Park, H. J. Kim, W. H. Hong, S. Lee and Y. S. Huh, *Nanoscale*, 2012, **4**, 4983–4988.
- 41 Z. S. Wu, W. Ren, D. W. Wang, F. Li, B. Liu and H. M. Cheng, *ACS Nano*, 2010, **4**, 5835–5842.
- 42 Z. Tang, C. Tang and H. Gong, *Adv. Funct. Mater.*, 2012, **22**, 1272–1278.